Accuracy of generalized gradient approximation functionals for density-functional perturbation theory calculations

L. H. He, Franklin Liu, G. Hautier, M. J. T. Oliveira, Miguel A. L. Marques,

F. D. Vila, J. J. Rehr, G. M. Rignanese, A. H. Zhou

Accuracy of generalized gradient approximation functionals for density-functional perturbation theory calculations

Lianhua He,[1] Fang Liu,[2] Geoffroy Hautier,[3,4] Micael J. T. Oliveira,[3,5] Miguel A. L. Marques,[3,6] Fernando D. Vila,[7] J. J. Rehr,[7] G.-M. Rignanese,[3,4] and Aihui Zhou[1]

[1]*LSEC, Institute of Computational Mathematics and Scientific/Engineering Computing, Academy of Mathematics and Systems Science, Chinese Academy of Sciences, Beijing 100190, China*

[2]*School of Applied Mathematics, Central University of Finance and Economics, Beijing 100081, China*

[3]*European Theoretical Spectroscopy Facility (ETSF)*

[4]*Institute of Condensed Matter and Nanosciences (IMCN), Université Catholique de Louvain, Chemin des Étoiles 8, 1348 Louvain-la-Neuve, Belgium*

[5]*Center for Computational Physics, University of Coimbra, Rua Larga, 3004-516 Coimbra, Portugal*

[6]*Institut Lumière Matière, UMR5306 Université Lyon 1-CNRS, Université de Lyon, F-69622 Villeurbanne Cedex, France*

[7]*Department of Physics, University of Washington, Seattle, Washington 98195, USA*

We assess the validity of various exchange-correlation functionals for computing the structural, vibrational, dielectric, and thermodynamical properties of materials in the framework of density-functional perturbation theory (DFPT). We consider five generalized-gradient approximation (GGA) functionals (PBE, PBEsol, WC, AM05, and HTBS) as well as the local density approximation (LDA) functional. We investigate a wide variety of materials including a semiconductor (silicon), a metal (copper), and various insulators (SiO_2 α-quartz and stishovite, $ZrSiO_4$ zircon, and MgO periclase). For the structural properties, we find that PBEsol and WC are the closest to the experiments and AM05 performs only slightly worse. All three functionals actually improve over LDA and PBE in contrast with HTBS, which is shown to fail dramatically for α-quartz. For the vibrational and thermodynamical properties, LDA performs surprisingly very well. In the majority of the test cases, it outperforms PBE significantly and also the WC, PBEsol and AM05 functionals though by a smaller margin (and to the detriment of structural parameters). On the other hand, HTBS performs also poorly for vibrational quantities. For the dielectric properties, none of the functionals can be put forward. They all (i) fail to reproduce the electronic dielectric constant due to the well-known band gap problem and (ii) tend to overestimate the oscillator strengths (and hence the static dielectric constant).

I. INTRODUCTION

The lattice-dynamical behavior ("the jiggling and wiggling of atoms," as Feynman poetically said [1]) determines many of the physical properties of solids: infrared, Raman, and neutron-diffraction spectra; specific heats, thermal expansion, and heat conduction; phenomena related to the electron-phonon interaction such as the resistivity of metals, superconductivity, the temperature dependence of optical spectra, etc. It is thus essential to be able to model accurately the lattice dynamics of materials to understand and predict many of their properties.

In the last three decades, theoretical condensed-matter physics and computational materials science have made considerable progress. Nowadays, many materials properties can be computed using *ab initio* quantum-mechanical techniques. Their only input information is the chemical composition and crystal structure of the material. The predictive power of *ab initio* computations has even started to be used to make materials design and predictions [2]. In the specific case of lattice-dynamical properties, a large number of *ab initio* calculations based on the linear-response theory of lattice vibrations have been made possible over the past twenty years by the achievements of density-functional theory [3] (DFT) and by the development of density-functional perturbation theory [4] (DFPT). Thanks to these theoretical and algorithmic advances, it is nowadays possible to obtain phonon dispersions on a fine grid of wave vectors covering the entire Brillouin zone, which can directly be compared with neutron-diffraction data. From the phonon frequencies, many of the above physical properties can be computed.

Within the framework of DFT, the many-body problem of interacting electrons in a static external potential is cast into a tractable problem of noninteracting electrons moving in an effective potential. The latter includes the external potential and the effects of the Coulomb interactions between the electrons, i.e., the so-called Hartree term, describing the electron-electron repulsion, and the exchange and correlation (XC) interactions, which includes all the many-body interactions. Modeling the XC interactions is the main difficulty of DFT. The simplest approximation is the local-density approximation [3,5] (LDA), which is based on the XC energy of the homogeneous electron gas and only requires the density at each point in space. A slightly more elaborate approach consists in using both the density and its gradient at each point in space in the so-called generalized gradient approximation (GGA).

For solids, the most commonly used GGA functional is the one proposed by Perdew, Burke, and Ernzherhof (PBE) [6]. It almost always overestimates the lattice constants of solids, while LDA consistently underestimates the volume. In both cases, the typical errors amount to 1%–2% of the lattice parameters. A series of alternative GGA functionals have recently been proposed to overcome this problem, as well as to obtain accurate surface energies for solids. One such functional is the AM05 functional [7], which combines

the LDA functional for bulklike regions with a local Airy approximation [8] for surfacelike regions. In contrast, the PBEsol [9] and Wu and Cohen (WC) [10] functionals can be seen as revised versions of PBE specifically adapted for solids. These three functionals (AM05, PBEsol, and WC) yield indeed lattice constants that are in excellent agreement with experiments [11]. More recently, the HTBS functional [12] has been proposed as an efficient compromise leading to good results on challenging problems requiring accuracy for both solids and molecules (e.g., the CO adsorption on noble metal surfaces). It is obtained by mixing two functionals: one performing well for atomization energies of molecules (the RPBE [13] functional) and one achieving very good accuracy for lattice constants in solids (WC).

These alternative functionals, which mainly focus on improving the modeling of the lattice constants, bond lengths and surface energies of solids, often compromise the accuracy for bulk total energies. It is therefore of interest to study how they perform when it comes to predicting properties governed by lattice dynamics (such as phonon frequencies, dielectric constants, and thermal properties) and that should be affected by both the accuracy in structural parameters and energy. It should be mentioned that the performance of PBE has already been tested for the phonon frequencies of a few selected solids [14–16]. A comparison of LDA, PBE, and an *ad hoc* functional (mixing 50% of the previous ones) has been proposed for copper focusing on the theoretical Debye-Waller factors [18]. The performance of the screened hybrid HSE functional has been studied for the lattice dynamics of group-IV elemental semiconductors and insulators using a finite differences approach [17]. More recently, the phonon dispersions of face-centered cubic metals (Cu, Ag, Au, Ni, Pd, Pt, Rh, and Ir) have also been investigated using the WC and PBEsol functionals [19].

In this paper, we consider five GGA functionals (PBE, PBEsol, WC, AM05, and HTBS) as well as the LDA to compute such properties using DFPT. We investigate a wide variety of materials including a semiconductor (silicon), a metal (copper), and various insulators (SiO_2 α-quartz and stishovite, $ZrSiO_4$ zircon, and MgO periclase). This allows us to assess the validity of the different XC functionals not only for structural properties (as commonly reported in the literature) but also for vibrational, thermodynamical, and dielectric properties.

This paper is organized as follows. Section II is devoted to the technical details of our calculations. Our main results are then presented in Sec. III: we present successively (III A) the structural properties, (III B) the phonon frequencies at Γ, (III C) the phonon dispersion curves, (III D) the volume dependence of the phonon frequencies, (III E) the thermodynamical properties, and (III F) the dielectric properties. Based on these results, a few general statements and considerations are given in Sec. IV. Finally, our most important findings are summarized in Sec. V.

II. TECHNICAL DETAILS

The *ab initio* calculations were performed using the ABINIT package [20] combined with the LIBXC library [21]. Total energies were computed using DFT, and phonon frequencies

TABLE I. Atomic valence configurations, core radii (r_c in a.u. for the different channels), and local channel (see text) of the pseudopotentials.

Atom	Configuration	r_c^s	r_c^p	r_c^d	Local
O	$2s^2 2p^4$	1.50	1.50	–	p
Mg	$3s^2 3p^0 3d^0$	2.10	2.50	2.50	s
Si	$3s^2 3p^2 3d^0$	1.73	1.90	2.03	d
Zr	$4s^2 4p^6 4d^2 5s^0$	1.95	1.75	1.90	d
Cu	$3d^{10} 4s^1 4p^0$	2.08	2.08	2.08	s

using DFPT. The exchange-correlation energy is evaluated within LDA using Perdew-Wang's parametrization [5] and GGA using the PBE [6], PBEsol [9], AM05 [7], WC [10], and HTBS [12] functionals. The interaction between the ions and valence electrons was described using Troullier-Martins norm-conserving pseudopotentials. These are generated by the atomic pseudopotentials engine [22] consistently with each XC functional. The reference configurations and core radii of our pseudopotentials (kept the same for all XC functionals) are reported in Table I. The plane-wave kinetic energy cutoff was set to 10 Ha for silicon, 30 Ha for zircon, α-quartz, and stishovite, 40 Ha for copper, 33 Ha for periclase. The Brillouin Zone (BZ) integrations were performed within Monkhorst-Pack (MP) scheme using $4 \times 4 \times 4$ grids for silicon, zircon, α-quartz, stishovite, periclase and using $6 \times 6 \times 6$ grids for copper. In order to deal with the possible convergence problems for copper, Gaussian smearing technique was employed with the smearing parameter set equal to 0.01 Hartree.

For a statistical analysis of the results obtained with the different XC functionals, we use the mean relative error (MRE, in percents) and the mean absolute relative error (MARE, in percents).

III. RESULTS AND ANALYSIS

A. Structural properties

We have studied in Table II the structural parameters (lattice constants but also bond lengths and angles) for the different compounds and functionals. The space group of silicon is $Fd\bar{3}m$. The Si atoms are located at $(\frac{1}{8}, \frac{1}{8}, \frac{1}{8})$ and $(\frac{7}{8}, \frac{7}{8}, \frac{7}{8})$ occupied the 8a Wyckoff sites [29]. In Table II, the optimal lattice constant of silicon calculated using different XC functionals are summarized and compared to the experimental value 5.431 Å [23].

The unit cell of α-quartz is trigonal (space group $P3_2 21$). It contains nine atoms: the Si atoms are located at $(u,0,0)$ on the 3a Wyckoff sites, while the O atoms are located at (x,y,z) on the 6c Wyckoff sites. Hence, four internal coordinates u, x, y, z are required, besides the two lattice constants a and c, in order to completely determine the structure. The theoretical value calculated here using the different XC functionals are reported in Table II. A comparison with the experimental values of Ref. [24] is also provided.

Stishovite has the rutile structure which is tetragonal (space group $P4_2/mnm$). The positions of the Si atoms are imposed by symmetry: they occupy the 2a Wyckoff sites located at

TABLE II. Calculated structural parameters of silicon, α-quartz, stishovite, zircon, periclase, and copper for various XC functionals. The theoretical results are compared to the experimental values taken from Ref. [23] for silicon, Ref. [24] for α-quartz, Ref. [25] for stishovite, Ref. [26] for zircon, Ref. [27] for periclase, and Ref. [28] for copper. The lattice constants (a and c) and the bond lengths (d) are expressed in Å, the bond angles are reported in degrees, whereas the internal parameters (u, v, x, y, and z) are dimensionless. The "good" (absolute relative error smaller than 0.5%) theoretical values are in bold and the "bad" (absolute relative error larger than 2%) values are underlined.

	LDA	PBE	PBEsol	AM05	WC	HTBS	Expt.		LDA	PBE	PBEsol	AM05	WC	HTBS	Expt.
Silicon															
a	5.382	5.467	**5.422**	**5.431**	**5.420**	**5.446**	5.431	d(Si-Si)	2.331	2.367	**2.348**	**2.352**	**2.347**	**2.358**	2.352
α-Quartz															
a	4.866	5.039	4.959	5.029	4.975	5.108	4.916	d(Si-O)	**1.600**	1.624	1.614	1.614	**1.613**	**1.620**	1.605
c	5.361	5.524	5.443	5.510	5.458	5.579	5.406		1.605	1.627	**1.618**	**1.617**	**1.616**	**1.620**	1.614
u	0.4666	0.4790	0.4725	0.4818	0.4748	0.5000	0.4697	$\angle$(Si-O-Si)	142.2	148.1	144.9	149.6	146.1	154.3	143.8
x	**0.4128**	**0.4155**	**0.4140**	0.4166	**0.4149**	0.4186	0.4135	$\angle$(O-Si-O)	**108.5**	109.4	**109.0**	109.5	**109.1**	110.0	108.8
y	0.2726	0.2511	0.2628	0.2458	0.2587	0.2093	0.2669		**109.3**	108.2	**108.6**	108.3	**108.6**	108.2	109.0
z	0.1153	0.1320	0.1225	0.1366	0.1259	0.1667	0.1191		**109.4**	108.9	**109.2**	108.9	**109.2**	108.2	109.2
									110.6	110.5	110.5	110.4	110.4	**110.3**	110.5
Stishovite															
a	4.155	4.246	**4.199**	4.206	**4.198**	4.217	4.180	d(Si-O)	1.753	1.777	**1.765**	**1.765**	**1.765**	1.771	1.758
c	**2.654**	2.694	**2.676**	2.675	**2.676**	2.685	2.667		1.792	1.844	**1.818**	1.822	**1.818**	1.827	1.810
u	**0.3057**	0.3070	**0.3062**	0.3064	**0.3062**	**0.3060**	0.3062	$\angle$(Si-O-Si)	98.4	98.6	**98.6**	98.5	98.6	98.6	98.7
									130.8	130.7	130.7	130.7	130.7	130.7	130.7
Zircon															
a	6.575	6.697	**6.631**	**6.642**	**6.629**	6.661	6.610	d(Zr-O)	**2.120**	2.162	2.138	2.143	2.138	2.148	2.124
c	5.900	**6.007**	5.949	5.956	5.949	**5.972**	6.001		2.252	**2.288**	2.268	2.267	2.270	2.272	2.287
u	0.0661	0.0666	0.0662	0.0664	0.0662	0.0663	0.0646	d(Si-O)	1.612	1.639	**1.627**	**1.628**	**1.626**	**1.633**	1.627
v	0.1953	0.1951	0.1949	0.1947	0.1951	0.1945	0.1967	$\angle$(Zr-O-Si)	98.9	99.0	99.0	**98.9**	99.0	**98.9**	98.7
									150.0	149.8	149.8	149.7	**149.9**	149.7	150.6
								$\angle$(Zr-O-Zr)	**111.1**	**111.2**	**111.2**	111.3	**111.2**	111.4	110.7
								$\angle$(O-Si-O)	97.2	97.1	97.1	97.0	97.1	97.0	97.8
									115.9	116.0	116.0	116.0	116.0	**116.0**	115.6
Periclase															
a	4.130	**4.231**	**4.194**	**4.194**	**4.192**	4.238	4.212	d(Mg-O)	2.065	**2.115**	2.097	2.097	**2.096**	2.119	2.106
Copper															
a	3.522	3.661	3.596	3.595	**3.599**	**3.599**	3.615	d(Cu-Cu)	2.512	2.589	2.543	2.542	**2.545**	**2.545**	2.556
MRE (%)	−0.79	1.31	0.27	0.99	0.43	2.31									
MARE (%)	1.35	2.15	0.82	2.32	1.17	5.28									

$(0,0,0)$ and $(\frac{1}{2},\frac{1}{2},\frac{1}{2})$. The O atoms are located at $(u,u,0),(1-u,1-u,0),(\frac{1}{2}-u,\frac{1}{2}+u,\frac{1}{2})$, and $(\frac{1}{2}+u,\frac{1}{2}-u,\frac{1}{2})$ on the $4f$ Wyckoff sites. The structure of stishovite is thus completely defined by the lattice constants a and c and a single internal coordinate u. In Table II, our calculated results are compared with experimental values [25].

Zircon has a conventional unit cell which is body-centered tetragonal (space group $I4_1/amd$). The positions of Zr and Si atoms are imposed by symmetry: they are located at $(0,\frac{3}{4},\frac{1}{8})$ and $(0,\frac{1}{4},\frac{3}{8})$ on the $4a$ and $4b$ Wyckoff sites, respectively. The O atoms occupy the $16h$ Wyckoff sites $(0,u,v)$, where u and v are internal parameters. Hence the structure of zircon is completely determined by the two lattice constants a and c and the two internal coordinates u and v. Table II summarizes our theoretical results for zircon together with the measurements of Ref. [26].

The space group of periclase is $Fm\bar{3}m$. The O atom occupies the $4a$ Wyckoff site $(0,0,0)$ and the Mg atom is located at $(\frac{1}{2},\frac{1}{2},\frac{1}{2})$ occupying the $4b$ Wyckoff sites. In Table II, the optimal lattice constant of periclase calculated using different XC functionals are summarized and compared to the experimental value 4.21 Å [27]. The space group of copper is $Fm\bar{3}m$. The Cu atom is located at $(0,0,0)$ occupied the $4a$

Wyckoff sites. The equilibrium lattice constants for copper are summarized in Table II.

A completely fair comparison between theoretical and experimental values is quite difficult to achieve. Indeed, in principle, the zero-point anharmonic expansion (ZPAE) should be taken into account. When comparing the performance of different XC functionals to predict the lattice constants of solids, a ZPAE correction is usually applied to the experimental results (see, e.g., Ref. [11]), leading to values typically 0.01–0.02 Å lower. However, while a ZPAE correction formula exists for cubic systems without any internal parameters, it is unfortunately not the case for all crystalline systems and, in particular, when internal parameters are involved. Therefore we decided not to apply such corrections in order to treat all the materials in the same way. Furthermore, for those materials (silicon, periclase, and copper) to which ZPAE corrections can be applied, we checked that the global trends discussed hereafter are essentially very similar whether or not the experimental results are corrected.

In Table II, we observe the well known general tendency of LDA and PBE to respectively underestimate and overestimate lattice constants. PBEsol and WC are the closest to the experimental lattice parameters. AM05 performs only slightly
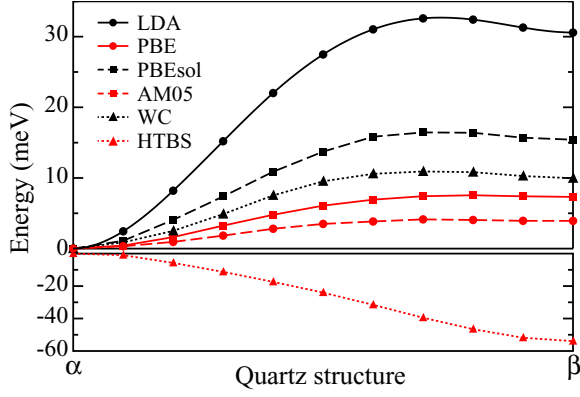
FIG. 1. (Color online) Energy for various quartz structures along the path from α- to β-quartz for the different XC functionals: LDA in solid black with circles, PBE in solid red (gray) with circles, PBEsol in dashed black with squares, AM05 in dashed red (gray) with squares, WC in dotted black with triangles, and HTBS in dotted red (gray) with triangles. HTBS fails to predict α-quartz as the stable phase.

worse than these functionals because of its larger errors for the α-quartz lattice parameter. These results are in agreement with a larger data set showing that WC, PBEsol, and AM05 perform similarly and better than LDA and PBE for lattice constants [11]. On the other hand, the HTBS functional is not performing better than LDA and PBE, and definitely does not reach the accuracy of the WC functional. The most dramatic failure of HTBS happens with α-quartz which cannot be stabilized and relaxes to β-quartz (or high quartz).

The latter is the stable polymorph of silica at higher temperature: at normal pressures, silica undergoes a structural transition from α- to β-quartz above $\sim$500 °C. In fact, these two forms of quartz are very similar, the relative positions of the atoms being only slightly shifted. The Si (respectively, O) atoms move from the 3a (respectively, 6c) and Wyckoff sites located at $(u,0,0)$ [respectively, (x,y,z)] in the α phase to the 3c (respectively, 6i) Wyckoff sites located at $(\frac{1}{2},0,0)$ [respectively, $(2y,y,\frac{1}{6})$] in the β phase. The number of internal coordinates is thus reduced from four (u, x, y, z) to one (y). The α- to β-quartz transition is displacive: the nearest neighbors of each atom remain the same, without breaking any of the chemical bonds. The relative positions of the atoms within the SiO$_4$ tetrahedra remain almost identical and the tetrahedra are not distorted very much. Instead, the SiO$_4$ tetrahedra get slightly twisted in a way that causes the unit cell, which is trigonal (space group $P3_221$) in α-quartz to become hexagonal (space group $P6_222$) in β-quartz.

In Fig. 1, we report the energy for various quartz structures (obtained by a linear interpolation of the internal coordinates and the lattice constants) along the path from α- to β-quartz for the different XC functionals. The α-quartz is found to be the stable phase with all functionals but HTBS, while β-quartz is a local minimum. With the HTBS functional, it is the β-quartz phase, which is stable, while the α-quartz phase is unstable.

We would like to point out that most of the studies evaluating the new GGA functionals [11] were carried out on highly-symmetric solids with few structural degrees of freedom (often only one lattice constant). The failure of HTBS

TABLE III. Fundamental frequencies of silicon (in cm^{-1}) with their symmetry assignments. The experimental values are taken from Ref. [31].

Mode	LDA	PBE	PBEsol	AM05	WC	HTBS	Expt.
T$_{1u}$	514	502	509	508	509	506	506
MRE (%)	1.53	-0.80	0.54	0.58	0.37	0.05	

for α-quartz shows that more complex structures (with internal parameters) should also be used to assess the performance of XC functionals in modeling structural parameters.

B. Phonon frequencies at the Γ point

We first compute the phonon frequencies at the Γ point of the Brillouin zone for all the materials using the different XC functionals. The calculations are performed using the corresponding theoretical equilibrium geometry (lattice parameters and internal coordinates) rather than the experimental one. As discussed by Baroni *et al.* [4], this is the most consistent choice when comparing with experimental data at low temperature. Furthermore, our aim is to evaluate the performance of the different XC functionals for predicting properties governed by lattice dynamics and it is more sensible to do so assuming that the experimental geometry is unknown. Indeed, when this is the case, it is mandatory to choose the theoretical equilibrium geometry for further calculations. Given the possible effects of the ZPAE and of the chosen pseudopotentials on the equilibrium geometry, conclusions should be drawn very carefully when comparing the different XC functionals. That is what we have tried to do in the following. Note that, due to the weak volume dependence of the Grüneisen parameter, it is straightforward to relate results at the equilibrium geometry with those, e.g., at the experimental geometry. This will be discussed in more detail in Sec. III D below.

In α-quartz, stishovite, zircon, and periclase, the nonvanishing components of the Born effective charge tensors [30] make it necessary to properly include the dipole-dipole interaction in the calculation of the interatomic force constants. In particular, the dipole-dipole contribution is found to be responsible for the splitting between the longitudinal and transverse optic (LO and TO, respectively) modes E$_u$ (perpendicular to c) and A$_u$ or A$_{2u}$ (parallel to c).

For silicon, the following irreducible representations of optical and acoustical zone-center modes can be obtained from group theory:

$$\Gamma = \underbrace{T_{1u}}_{\text{Raman}} \oplus \underbrace{T_{1u}}_{\text{Acoustic}} \, .$$

Our results for silicon are reported in Table III and compared with experimental data [31].

They are in line with the conclusions of Ref. [14] regarding the evolution of the phonon frequencies with the lattice constant. LDA (respectively, PBE) underestimates (overestimates) the lattice constants and overestimates (respectively, underestimates) the phonon frequency. The other XC functionals produce lattice constants and phonon frequencies in excellent agreement with experiment. In fact, the results are very good

TABLE IV. Fundamental frequencies of α-quartz (in cm^{-1}) with their symmetry assignments. The experimental values are extrapolated from the temperature-dependent values provided by Ref. [32] (for the six highest E modes and the A_2 modes) and by Ref. [33] (two lowest E modes and the A_1 modes) using a $\omega(T) = \omega_0 + aT^{1.8}$ law as advocated in the latter paper. The "good" (absolute relative error smaller than 2%) theoretical values are in bold and the "bad" (absolute relative error larger than 5%) values are underlined.

Mode	LDA	PBE	PBEsol	AM05	WC	HTBS	Expt.
Raman							
$A_1(1)$	**215**	146	182	129	170	29	219
$A_1(2)$	344	343	341	346	344	**352**	358
$A_1(3)$	454	429	438	429	437	423	469
$A_1(4)$	**1069**	1043	1055	**1062**	1058	**1063**	1082
Infrared							
$A_2(TO1)$	351	**358**	350	**366**	**355**	396	361
$A_2(LO1)$	374	377	372	**383**	376	396	385
$A_2(TO2)$	486	451	467	447	464	410	499
$A_2(LO2)$	540	514	523	513	523	496	553
$A_2(TO3)$	**764**	742	752	752	753	751	778
$A_2(LO3)$	**781**	748	762	756	761	751	791
$A_2(TO4)$	**1063**	1029	1044	1049	1047	1047	1072
$A_2(LO4)$	**1226**	1196	**1207**	**1215**	**1211**	**1215**	1230
$E_u(TO1)$	129	113	119	110	117	105	133
$E_u(LO1)$	129	113	119	110	117	105	133
$E_u(TO2)$	258	247	250	245	249	243	269
$E_u(LO2)$	259	247	251	246	250	243	269
$E_u(TO3)$	381	377	376	379	378	384	394
$E_u(LO3)$	391	383	384	385	386	384	402
$E_u(TO4)$	441	416	425	415	425	401	453
$E_u(LO4)$	498	477	483	478	484	470	512
$E_u(TO5)$	**685**	654	667	660	666	652	698
$E_u(LO5)$	**688**	655	669	661	668	652	701
$E_u(TO6)$	**786**	751	767	759	766	750	799
$E_u(LO6)$	**799**	763	779	771	778	762	812
$E_u(TO7)$	**1054**	1025	1038	1044	1041	1044	1066
$E_u(LO7)$	**1217**	1188	1200	**1207**	**1204**	**1209**	1227
$E_u(TO8)$	**1140**	1126	1130	**1144**	**1136**	**1152**	1158
$E_u(LO8)$	**1137**	1125	1128	**1143**	**1134**	**1152**	1155
MRE (%)	−2.22	−6.92	−5.10	−6.61	−5.23	−8.79	
MARE (%)	2.22	6.92	5.10	6.71	5.23	9.68	

TABLE V. Fundamental frequencies of stishovite (in cm^{-1}) with their symmetry assignments. The experimental values are taken from Ref. [34] for the Raman modes and Ref. [35] for the infrared modes. The "good" (absolute relative error smaller than 2%) theoretical values are in bold and the "bad" (absolute relative error larger than 5%) values are underlined.

Mode	LDA	PBE	PBEsol	AM05	WC	HTBS	Expt.
Raman							
A_{1g}	**748**	715	734	732	732	727	751
B_{1g}	220	222	218	220	218	219	234
B_{2g}	945	902	923	920	924	916	964
E_g	**578**	552	565	564	564	560	586
Infrared							
$A_{2u}(TO)$	**643**	619	632	633	630	629	650
$A_{2u}(LO)$	1047	1013	1028	1028	1028	1023	950
$E_u(TO1)$	**465**	422	445	444	446	441	470
$E_u(LO1)$	**563**	527	545	543	546	539	565
$E_u(TO2)$	**577**	529	555	550	555	548	580
$E_u(LO2)$	**701**	672	684	684	686	680	700
$E_u(TO3)$	**819**	791	**804**	**805**	803	800	820
$E_u(LO3)$	1032	989	**1011**	**1009**	**1011**	**1004**	1020
Silent							
$B_{1u}(1)$	383	367	374	374	374	372	–
$B_{1u}(2)$	749	718	734	732	734	728	–
A_{2g}	600	573	581	582	584	577	–
MRE (%)	−0.11	−4.72	−2.48	−2.59	−2.49	−3.14	
MARE (%)	2.03	5.82	3.85	3.95	3.86	4.42	

significantly for the different XC functionals. LDA shows the smallest relative errors, which are actually two to three times smaller than for the other XC functionals. LDA, PBE, PBEsol, and WC are found to systematically underestimate the phonon frequencies. It is almost systematically the case for AM05. HTBS leads to the worst results since they refer to the β-quartz.

For stishovite, the following irreducible representations of optical and acoustical zone-center modes can be obtained from group theory:

$$\Gamma = \underbrace{A_{1g} \oplus B_{1g} \oplus B_{2g} \oplus E_g}_{\text{Raman}} \oplus \underbrace{A_{2u} \oplus 3E_u}_{\text{IR}}$$
$$\oplus \underbrace{A_{2u} \oplus E_u}_{\text{Acoustic}} \oplus \underbrace{2B_{1u} \oplus A_{2g}}_{\text{Silent}}.$$

In Table V, we show the calculated and experimental values [34,35] for the frequency of each mode at the Γ point of stishovite.

While PBEsol and WC provide the best structural properties, it is again LDA which leads to the smallest relative error on the phonon frequencies. It is worth mentioning that all the alternative GGA functionals (PBEsol, AM05, WC, and HTBS) improve compared to PBE, PBEsol and WC providing the best results (though worse than LDA). None of the functionals present a systematic trend (under- or overestimation) in the errors.

For zircon, the theoretical group analysis provides the following irreducible representations of optical and acoustical

(absolute relative error smaller than 2%) for all the XC functionals including LDA and PBE. Thus this system is not really meaningful on its own to discriminate among them.

For α-quartz, the theoretical group analysis predicts the following irreducible representations of optical and acoustical zone-center modes:

$$\Gamma = \underbrace{4A_1 \oplus 9E}_{\text{Raman}} \oplus \underbrace{4A_2 \oplus 8E}_{\text{IR}} \oplus \underbrace{A_2 \oplus E}_{\text{Acoustic}}.$$

Table IV summarizes our results for α-quartz, and compares with experimental results at 0 K [32,33]. Note that the results for the HTBS functional refer to the β-quartz.

In contrast with silicon, it is not obvious to correlate the performance for phonon frequencies with the structural properties. However, the relative errors vary much more

TABLE VI. Fundamental frequencies of zircon (in cm^{-1}) with their symmetry assignments. The experimental values are taken from Ref. [36]. The "good" (absolute relative error smaller than 2%) theoretical values are in bold and the "bad" (absolute relative error larger than 5%) values are underlined.

Mode	LDA	PBE	PBEsol	AM05	WC	HTBS	Expt.
Raman							
$A_{1g}(1)$	**437**	415	425	423	426	422	439
$A_{1g}(2)$	**960**	920	940	936	941	933	974
$B_{1g}(1)$	222	201	**212**	**210**	**213**	209	214
$B_{1g}(2)$	**388**	368	378	375	379	375	393
$B_{1g}(3)$	626	603	612	610	614	607	–
$B_{1g}(4)$	**1002**	956	981	977	981	975	1008
B_{2g}	256	256	253	256	254	254	266
$E_g(1)$	193	191	190	192	191	191	201
$E_g(2)$	**224**	213	218	218	218	217	225
$E_g(3)$	**362**	322	343	334	345	333	357
$E_g(4)$	535	521	525	527	526	524	547
$E_g(5)$	910	867	889	886	890	884	–
Infrared							
$A_{2u}(TO1)$	345	315	330	327	331	327	338
$A_{2u}(LO1)$	**471**	449	460	459	460	457	480
$A_{2u}(TO2)$	**596**	572	582	580	584	577	608
$A_{2u}(LO2)$	**640**	611	624	621	626	618	647
$A_{2u}(TO3)$	967	921	946	942	946	940	989
$A_{2u}(LO3)$	1084	1039	1061	1059	1063	1055	1108
$E_u(TO1)$	279	252	267	263	268	262	287
$E_u(LO1)$	338	331	333	334	334	332	352
$E_u(TO2)$	376	355	365	362	366	361	389
$E_u(LO2)$	**416**	391	404	400	405	398	419
$E_u(TO3)$	**422**	413	414	415	416	413	430
$E_u(LO3)$	**463**	444	452	452	452	449	471
$E_u(TO4)$	856	813	836	832	836	830	885
$E_u(LO4)$	**1017**	972	994	990	996	987	1035
Silent							
B_{1u}	124	135	127	132	128	134	–
A_{2g}	243	242	240	242	241	241	–
A_{1u}	391	388	387	389	388	389	–
$B_{2u}(1)$	562	541	551	550	551	547	–
$B_{2u}(2)$	933	892	913	908	914	905	–
MRE (%)	−1.49	−6.36	−4.08	−4.45	−3.84	−4.82	
MARE (%)	2.09	6.36	4.08	4.45	3.84	4.82	

zone-center modes:

$$\Gamma = \underbrace{2A_{1g} \oplus 4B_{1g} \oplus B_{2g} \oplus 5E_g}_{\text{Raman}} \oplus \underbrace{3A_{2u} \oplus 4E_u}_{\text{IR}}$$
$$\oplus \underbrace{A_{2u} \oplus E_u}_{\text{Acoustic}} \oplus \underbrace{B_{1u} \oplus A_{2g} \oplus A_{1u} \oplus 2B_{2u}}_{\text{Silent}} .$$

Table VI summarizes our results for zircon and compares with experimental results [36]. The dipole-dipole contribution is found to be responsible for the splitting between the longitudinal optical (LO) and transverse optic (TO) modes E_u and A_{2u} at the Γ point.

As for stishovite, there is no clear correlation between the performance with respect to the prediction of the structural properties and the quality of the phonon frequencies. In the
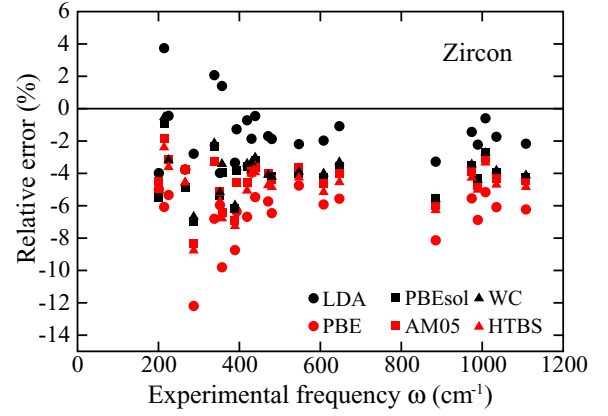

FIG. 2. (Color online) Relative error with respect to the experimental frequencies of zircon for the different XC functionals: LDA (black circles), PBE [red (gray) circles], PBEsol (black squares), AM05 [red (gray) squares], WC (black triangles), and HTBS [red (gray) triangles].

case of zircon, all the GGA functionals tend to underestimate the phonon frequencies, whereas there is no systematic trend for LDA. Once again, PBE is performing the worst, while PBEsol and WC are the best GGAs. These conclusions are clearly seen in Fig. 2, which shows the relative errors for each phonon mode as a function of the experimental frequency. A similar graph (not shown here for sake of brevity) is obtained for both SiO$_2$ phases (α-quartz and stishovite). It is also interesting to note that all functionals tend to underestimate the experimental data at high frequency.

For periclase, the following irreducible representations of optical and acoustical zone-center modes can be obtained from group theory:

$$\Gamma = \underbrace{T_{1u}}_{\text{IR}} \oplus \underbrace{T_{1u}}_{\text{Acoustic}} .$$

Table VII shows our results for periclase and experimental values [37].

In periclase, the worst results are obtained with HTBS. LDA and PBE perform slightly better (with a similar accuracy), the best performances being obtained with PBEsol, WC, and AM05 in contrast with the observations for the other oxides (quartz, stishovite, and zircon). Note that the LDA systematically overestimates while all the GGAs underestimate the phonon frequencies.

For copper, all the phonon frequencies at the Γ point are zero. There are only three acoustic since there is one atom per

TABLE VII. Fundamental frequencies of periclase (in cm^{-1}). The experimental values are taken from Ref. [37]. The "good" (absolute relative error smaller than 2%) theoretical values are in bold and the "bad" (absolute relative error larger than 5%) values are underlined.

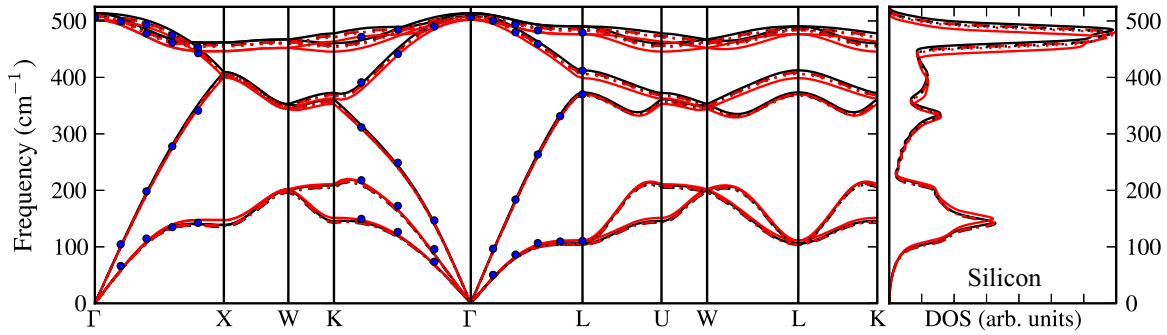| Mode	LDA	PBE	PBEsol	AM05	WC	HTBS	Expt.
Infrared							
$T_{1u}(TO1)$	420	373	**391**	**390**	**391**	370	396
$T_{1u}(LO1)$	727	686	**698**	**699**	**700**	684	710
MRE (%)	4.23	−4.59	−1.48	−1.53	−1.34	−5.11	
MARE (%)	4.23	4.59	1.48	1.53	1.34	5.11	

FIG. 3. (Color online) Phonon band structure and density of states of silicon computed using the different XC functionals: LDA in solid black, PBE in solid red (gray), PBEsol in dashed black, AM05 in dashed red (gray), WC in dotted black, and HTBS in dotted red (gray). The experimental data from Refs. [31,38] are also reported as blue (black) circles.

unit cell. An analysis of the fundamental frequencies at other selected points of the Brillouin zone will be given in Sec. III C.

Globally, LDA is the functional that performs the best among all, while PBEsol and WC are the best among the GGAs. The worst result is obtained with HTBS for the $A_1(1)$ mode of quartz (29 cm^{-1} instead of 219 cm^{-1}). This tremendous error comes from the wrong prediction of the stable structure with this functional (β- instead of α-quartz). Even after the exclusion of the quartz data, the HTBS functional still performs significantly worse than LDA, WC, PBEsol, and AM05. Note also that there is no systematic trend (under- or overestimation) in the relative errors obtained with the different functionals.

C. Phonon-dispersion relations

We also compute the phonon band structure and density of states (DOS) of the different materials using the different XC functionals. Our results are presented in Figs. 3–8. Available experimental data are also reported for comparison. The agreement is qualitatively very good though some significant discrepancies are present (especially at higher frequencies) independently of the XC functional. Given the variations existing in the experimental data and the typical error bars, it

did not seem meaningful to us to define a quantitative measure of the agreement between theory and experiment in order to discriminate between the different XC functionals.

For the oxides (α-quartz, stishovite, zircon, and periclase), it is reasonable to say that the LDA seems to perform slightly better than all the GGA functionals. In contrast, for copper, LDA shows the largest discrepancies while PBE seems to perform the best. This can also be seen in Table VIII where the fundamental frequencies at selected points of the Brillouin zone have been reported.

We would like to point out that our results for copper are shifted up by 5%–7% compared to those of Ref. [19] in which the WC and PBEsol frequencies match the experimental data better than LDA or PBE. There are several differences between the two calculations which may explain this discrepancy. In Ref. [19], the phonon frequencies are computed at the equilibrium lattice constant at $T = 296$ K, while we use the one at $T = 0$. This probably accounts for 1%–2% difference, as observed experimentally [47] and as discussed below. Furthermore, the calculations of Ref. [19] are based on the projector augmented wave (PAW) method, while ours rely on the use of norm-conserving pseudopotentials. It is interesting to point out that despite the equilibrium lattice constants at $T = 0$ K are in excellent agreement (at most 0.5%
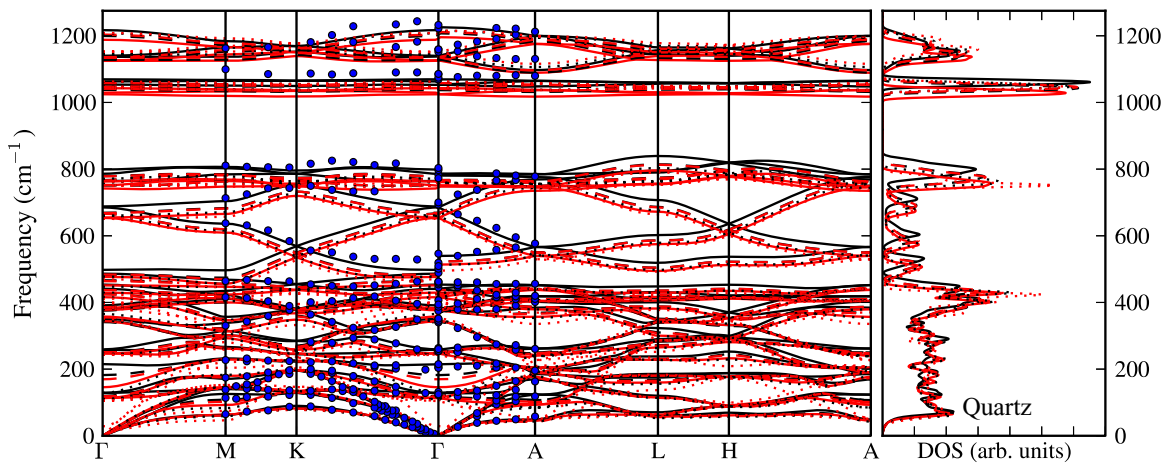

FIG. 4. (Color online) Phonon band structure and density of states of quartz computed using the different XC functionals: LDA in solid black, PBE in solid red (gray), PBEsol in dashed black, AM05 in dashed red (gray), WC in dotted black, and HTBS in dotted red (gray). The experimental data from Refs. [39–41] are also reported as blue (black) circles.
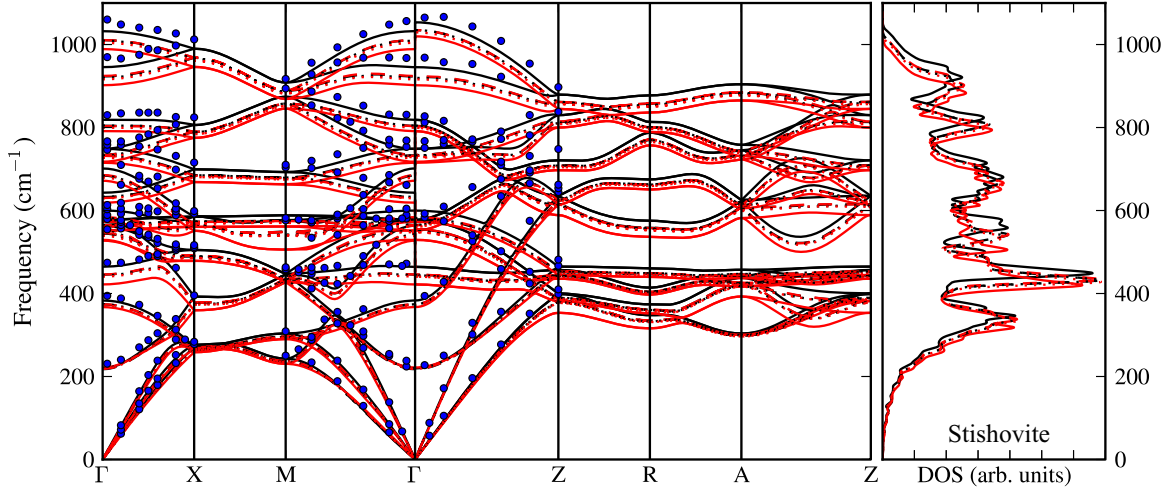
FIG. 5. (Color online) Phonon band structure and density of states of stishovite computed using the different XC functionals: LDA in solid black, PBE in solid red (gray), PBEsol in dashed black, AM05 in dashed red (gray), WC in dotted black, and HTBS in dotted red (gray). The experimental data from Ref. [42] are also reported as blue (black) circles.
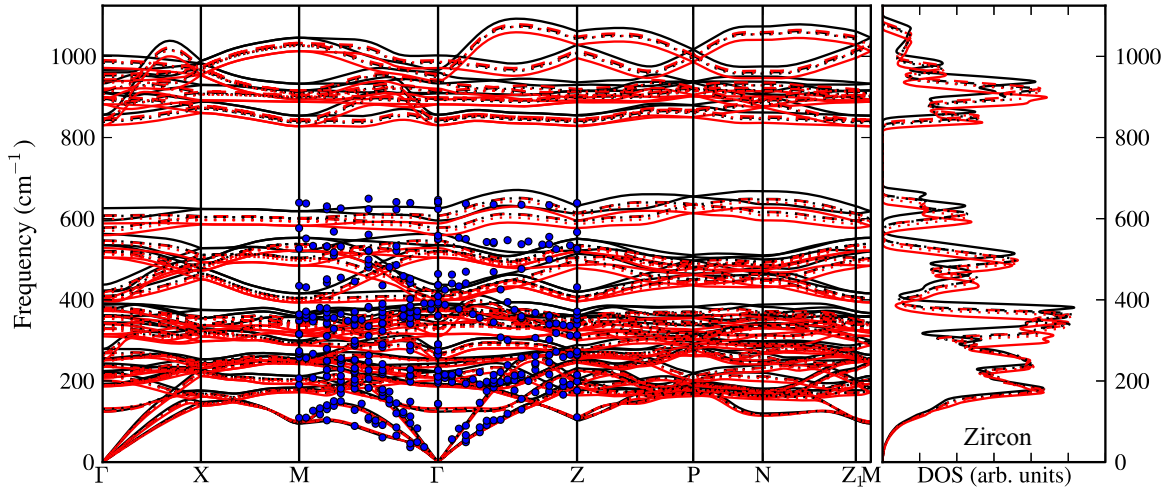

FIG. 6. (Color online) Phonon band structure and density of states of zircon computed using the different XC functionals: LDA in solid black, PBE in solid red (gray), PBEsol in dashed black, AM05 in dashed red (gray), WC in dotted black, and HTBS in dotted red (gray). The experimental data from Refs. [43–45] are also reported as blue (black) circles.
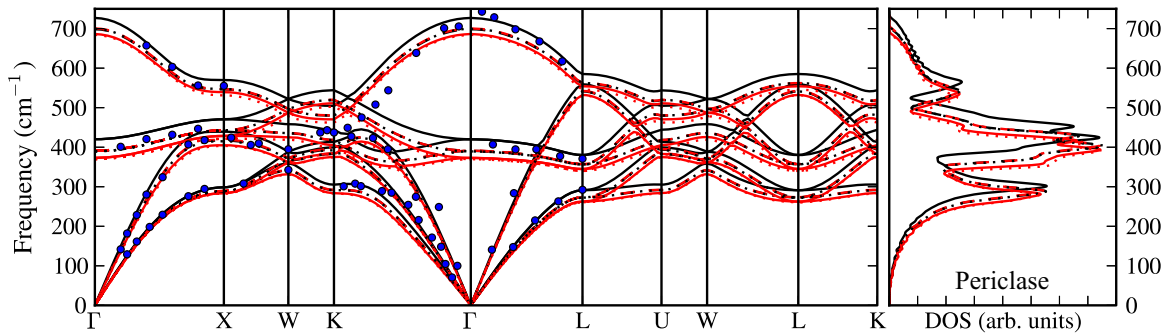

FIG. 7. (Color online) Phonon band structure and density of states of periclase computed using the different XC functionals: LDA in solid black, PBE in solid red (gray), PBEsol in dashed black, AM05 in dashed red (gray), WC in dotted black, and HTBS in dotted red (gray). The experimental data from Ref. [37] are also reported as blue (black) circles.
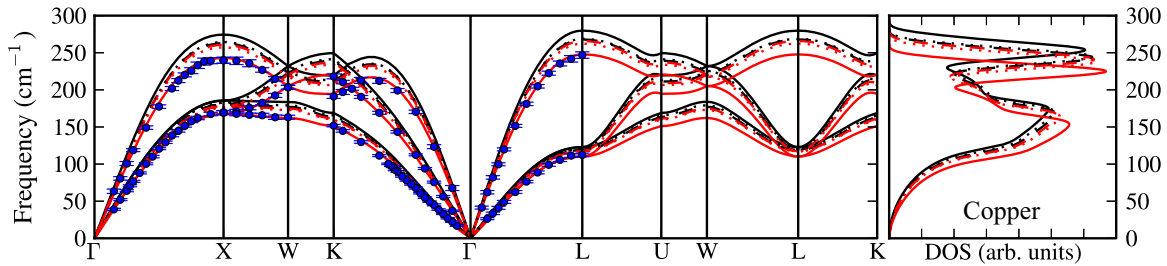
FIG. 8. (Color online) Phonon band structure and density of states of copper computed using the different XC functionals: LDA in solid black, PBE in solid red (gray), PBEsol in dashed black, AM05 in dashed red (gray), WC in dotted black, and HTBS in dotted red (gray). The experimental data (with error bars) from Ref. [46] are also reported as blue (black) circles.

discrepancy), the phonon frequencies may show important differences. This emphasizes the importance of assessing the accuracy of pseudopotentials by comparing with all-electron results not only for structural but also for dynamical properties.

When looking at the phonon DOS in Figs. 3–8, it looks as if it were simply shifted when changing the XC functional (with LDA and PBE at the upper and lower ends and all the other functionals falling in the middle almost on top of one another). This is confirmed by computing the different moments of the phonon DOS: the average frequency $\bar{\omega}$ (1st moment) is much more dependent on the XC functional than all higher moments. In Table IX, we show the average frequency $\bar{\omega}$ and the standard deviation σ (second moment) extracted from the phonon DOS computed at the theoretical lattice constant of the different materials using the different XC functionals. Higher moments (not reported for sake of brevity) do not vary much with the XC functional.

D. Volume dependence of the phonon frequencies

The different XC functionals lead to different lattice constants and the latter influence the computed frequency. Here, we study the volume dependence of the average frequency ($\bar{\omega}$) for the different XC functionals.

We can distinguish an indirect effect through the equilibrium lattice constant from the direct effect (for a fixed lattice constant). Indeed, the average frequency changes quite strongly with the lattice constants as illustrated in Fig. 9 for periclase and copper: an increase of the lattice constant by

0.2 Å can induce a decrease of $\bar{\omega}$ by 80–100 cm^{-1}. In contrast, the direct effect is rather small at most 15 cm^{-1} between the two extreme results (produced by LDA and PBE). To illustrate this point, let us consider periclase. In Table IX, we have $\bar{\omega} = 413$ cm^{-1} using LDA and 383 cm^{-1} using PBE. This looks like a decrease by 30 cm^{-1}. However, these values are calculated for two different lattice constants $a = 4.13$ Å for LDA and $a = 4.23$ Å for PBE. If the functional were changed from LDA to PBE while keeping the LDA equilibrium lattice constant, the average frequency would actually increase by 13 cm^{-1} (from 413 to 426 cm^{-1}). This is the direct effect of the XC functional. Whereas, the indirect effect (due to the change from LDA to PBE equilibrium lattice constant) produces a decrease by 43 cm^{-1}.

The lattice (or volume) dependence of the average frequency is measured by the corresponding Grüneisen parameter $\gamma = -\frac{d \ln \bar{\omega}}{d \ln V}$, which is also reported in Fig. 9. Interestingly enough, all functionals produce very comparable Grüneisen parameters. For periclase, $\gamma \simeq 1.47$–1.57 is comparable to the measured values ranging from 1.49 [48] to 1.60 [49]. For copper, $\gamma \simeq 2.08$–2.34 is in very good agreement with the reported experimental value of $\gamma \simeq 2$ [49–51] and previous theoretical results [18]. This weak variation with the XC functional might be exploited as follows. If the average frequencies were known for various XC functionals at a given lattice constant value, computing the volume dependence of the frequency for just one of those functionals would be

TABLE VIII. Fundamental frequencies of copper (in cm^{-1}) at selected point of the Brillouin Zone with their symmetry assignments. The experimental values are taken from Ref. [46]. The "good" (absolute relative error smaller than 2%) theoretical values are in bold and the "bad" (absolute relative error larger than 5%) values are underlined.

Mode	LDA	PBE	PBEsol	AM05	WC	HTBS	Expt.
X_T	<u>186</u>	**168**	<u>180</u>	<u>183</u>	<u>178</u>	176	169
X_L	<u>275</u>	**243**	<u>263</u>	<u>265</u>	<u>261</u>	<u>257</u>	240
W_Λ	<u>184</u>	**162**	<u>177</u>	<u>179</u>	<u>175</u>	<u>173</u>	163
W_Π	<u>232</u>	**205**	<u>223</u>	<u>225</u>	<u>220</u>	<u>218</u>	203
L_T	<u>123</u>	**110**	<u>119</u>	<u>121</u>	117	117	112
L_L	<u>280</u>	**248**	<u>268</u>	<u>269</u>	<u>266</u>	<u>262</u>	247
MRE (%)	12.50	−0.06	8.21	9.38	6.99	5.88	
MARE (%)	12.50	0.94	8.21	9.38	6.99	5.88	

TABLE IX. Average frequency ($\bar{\omega}$) and standard deviation (σ) of the phonon density of states calculated at the theoretical lattice constant for silicon, α-quartz, stishovite, zircon, periclase, and copper for the different XC functionals. $\bar{\omega}$ and σ are expressed in cm^{-1}.

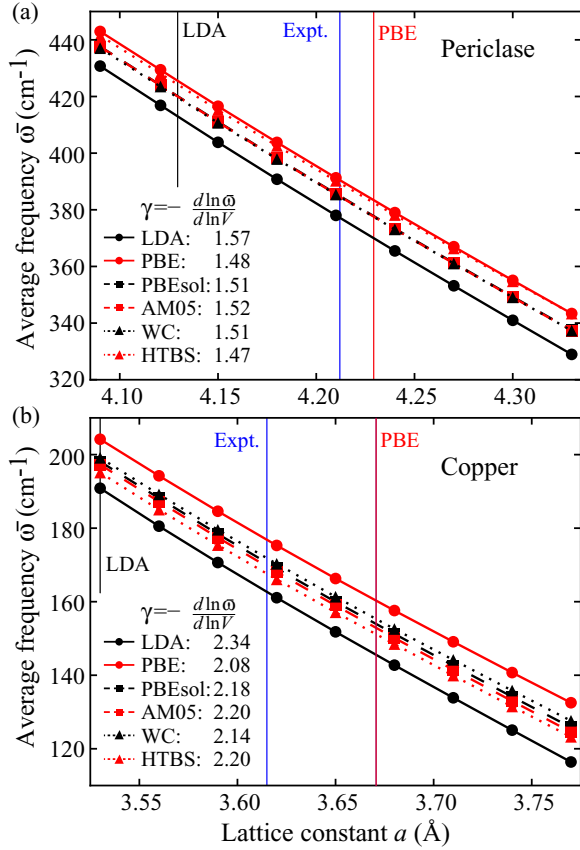|		LDA	PBE	PBEsol	AM05	WC	HTBS
Silicon	$\bar{\omega}$	330	324	327	327	326	325
	σ	146	139	145	145	144	144
α-Quartz	$\bar{\omega}$	557	539	545	546	544	541
	σ	359	352	356	357	360	361
Stishovite	$\bar{\omega}$	580	552	566	566	564	562
	σ	207	201	204	204	204	203
Zircon	$\bar{\omega}$	480	458	468	470	467	465
	σ	294	281	288	288	287	286
Periclase	$\bar{\omega}$	413	383	392	393	392	379
	σ	118	113	114	114	114	112
Copper	$\bar{\omega}$	183	163	176	175	178	173
	σ	55	49	53	52	53	52

FIG. 9. (Color online) Variation of the average frequency $\bar{\omega}$ (in cm^{-1}) of (a) periclase and (b) copper as a function of the lattice constant a (in Å) computed using the different XC functionals: LDA in solid black, PBE in solid red (gray), PBEsol in dashed black, AM05 in dashed red (gray), WC in dotted black, and HTBS in dotted red (gray). The vertical lines indicate the experimental lattice constant taken from Refs. [27,28], and the two extreme PBE and LDA lattice constants for periclase and copper, respectively.

sufficient to provide a reasonable extrapolation scheme for $\bar{\omega}(a)$ for any of the XC functionals.

E. Thermodynamical properties

The vibrational entropy of a solid can be obtained from its phonon distribution. This quantity is of importance for the *ab initio* assessment of solid phase stability. The entropy $S(T)$ at temperature T is first computed within the harmonic approximation [52] for the different materials in their equilibrium structural configuration. In Table X, the entropy at 298 K calculated using the various XC functionals is compared with the experimental measurements [53–55]. All the results are in good agreement with experiments apart from those for zircon [56]. We note that the LDA functional presents the best results. AM05, PBEsol, and WC are the best among the GGAs, while HTBS is the worst.

In any case, the absolute error on the contribution of the vibrational entropic term to the free energy (TS) is around 2 to 3 meV/atom. This is much smaller than the typical errors on the energy term [57,58].

TABLE X. Calculated entropy (in J/mol/K) at 298 K of silicon, α-quartz, stishovite, zircon, periclase, and copper for various XC functionals. The theoretical results are compared to the experimental values taken from Refs. [53–55]. The "good" (absolute relative error smaller than 3%) theoretical values are in bold and the "bad" (absolute relative error larger than 5%) values are underlined.

	LDA	PBE	PBEsol	AM05	WC	HTBS	Expt.
Silicon							
	19.41	19.56	19.67	19.61	19.67	19.71	18.81[a], 18.80[b]
α-Quartz							
	42.40	44.32	43.76	43.86	44.48	44.95	41.44[a], 43.40[b]
Stishovite							
	24.56	<u>26.84</u>	25.72	25.66	25.81	26.03	24.94[c]
Zircon							
	<u>90.15</u>	<u>94.86</u>	<u>92.77</u>	<u>92.38</u>	<u>93.20</u>	<u>93.41</u>	84.50[b]
Periclase							
	25.71	28.59	**27.59**	**27.52**	**27.63**	28.96	26.95[a], 26.90[b]
Copper							
	<u>30.21</u>	**32.94**	31.06	31.34	30.85	31.57	33.15[a], 33.10[b]
	−0.83	5.68	2.83	2.79	3.18	4.77	MRE (%)
	4.52	5.87	4.90	4.58	5.47	6.34	MARE (%)

[a]Reference [53].
[b]Reference [54].
[c]Reference [55].

In the following, we take periclase and copper as examples to study how XC functionals impact other thermal properties. First, the free energy $F(a,T)$ [$F(V,T)$] at temperature T and lattice constant a [volume V] are computed within the quasiharmonic approximation [4]. By fitting the results for the free energy to the third-order Birch-Murnaghan equation of state [59], we can obtain the variation in temperature of the equilibrium lattice constants $a_0(T)$ [volumes $V_0(T)$], the bulk modulus B_0, and the pressure derivative of the bulk modulus B'. The linear thermal expansion $\varepsilon(T)$ is then given by

$$\varepsilon(T) = \frac{a_0(T) - a_0(T_c)}{a_0(T_c)},$$

where $T_c = 298$ K is the reference temperature. Finally, the coefficient of linear thermal expansion is obtained as

$$\alpha(T) = \frac{1}{a_0(T_c)} \frac{da_0(T)}{dT}.$$

Figures 10 and 11 show the results for (a) $\varepsilon(T)$ (expressed as a percentage), (b) $\alpha(T)$, and (c) $B_0(T)$ using various XC functionals.

For periclase, the anharmonic effects are very important. Thus, empirical corrections are necessary to obtain good thermodynamic properties over a wide temperature range [67,68]. Here, we did not go through this special procedure that would not allow to discriminate the different XC functionals. So, the calculations of ε, α, and B_0 were limited to temperatures lower than 1000 K. Ideally, it would be better to focus on even smaller temperatures but very few data are available. At low temperature, LDA seems to produce the best results. In contrast, like for the frequency at Γ, the HTBS results fall outside the LDA-PBE range on the PBE side, leading to the worst agreement with experiments.

For copper, LDA (respectively, PBE) underestimates (respectively, overestimates) the thermal expansion (ε and α) while all the other GGAs show an excellent agreement with the experimental results. For the bulk modulus, PBE underestimates compared to the measured data, while all other functionals overestimate. HTBS performs the best and LDA is the worst with $\sim 5\%$ and $\sim 20\%$ discrepancy, respectively. All other GGAs (including PBE) show an error of $\sim 7\%$–8% compared to experiments.

F. Dielectric permittivity tensors

Finally, we turn to the calculation of the electronic (ϵ_∞) and static (ϵ_0) permittivity tensors. The electronic (ion-clamped) dielectric permittivity tensor is related to the second-order derivatives of the energy with respect to the macroscopic electric field. The static dielectric permittivity tensor also includes the polarization coming from the ionic displacements. It is obtained by adding the contributions of different modes to ϵ_∞ as follows:

$$
\begin{aligned}
\epsilon^0_{\alpha\beta} &= \epsilon^\infty_{\alpha\beta} + \sum_m \Delta\epsilon_{m,\alpha\beta} \\
&= \epsilon^\infty_{\alpha\beta} + \frac{4\pi}{\Omega_0} \sum_m \frac{S_{m,\alpha\beta}}{\omega_m^2},
\end{aligned}
\tag{1}
$$

where Ω_0 is the volume of the primitive unit cell and $S_{m,\alpha\beta}$ is the mode-oscillator strength.

The electronic (ϵ_∞) and static (ϵ_0) permittivity tensors, as well as the contributions of the individual modes $\Delta\epsilon_m$, are reported in Table XI for α-quartz, stishovite, zircon, and periclase. Due to the symmetry of the different crystalline systems, they have two different components parallel ($\parallel$) and perpendicular ($\perp$) to the c axis for the first three materials [α-quartz (trigonal), stishovite, and zircon (tetragonal)], while the tensor is isotropic for periclase (cubic). In stishovite and zircon (respectively, α-quartz), the phonon mode contributions to $\epsilon_0^{\parallel}$ come from the three IR-active A_{2u} (respectively, A_2) modes, while the contributions to $\epsilon_0^{\perp}$ come from the four IR-active E_u (respectively, E) modes. In periclase, the contribution arises from the T_{1u} mode. For α-quartz, the experimental values (at 298 K) are taken from Ref. [32], except for the two lowest E modes which are from Ref. [69]. For stishovite, the measurements are those of Ref. [70]. For zircon, the reported experimental values are from Ref. [71] for the parallel components (values at 295 K), and from Ref. [72] for the perpendicular components. For periclase, the measurements are those of Ref. [73].

The theoretical values of ϵ_∞ are larger than the experimental ones by about 68%, as often found in DFT. The only exception is α-quartz for which the values obtained with the different GGAs are much closer to the experimental values and tend to slightly underestimate it (note that HTBS results actually refer to β-quartz). In fact, the overestimation of the electronic dielectric constant can be related to the band-gap problem of DFT, and, since the different XC functionals produce similar incorrect band gaps, there is not a significant difference among the different results.

The contributions of each individual mode $\Delta\epsilon_m$ depend on the volume ($\Delta\epsilon_m \propto \Omega_0^{-1}$), the oscillator strength ($\Delta\epsilon_m \propto S_m$)
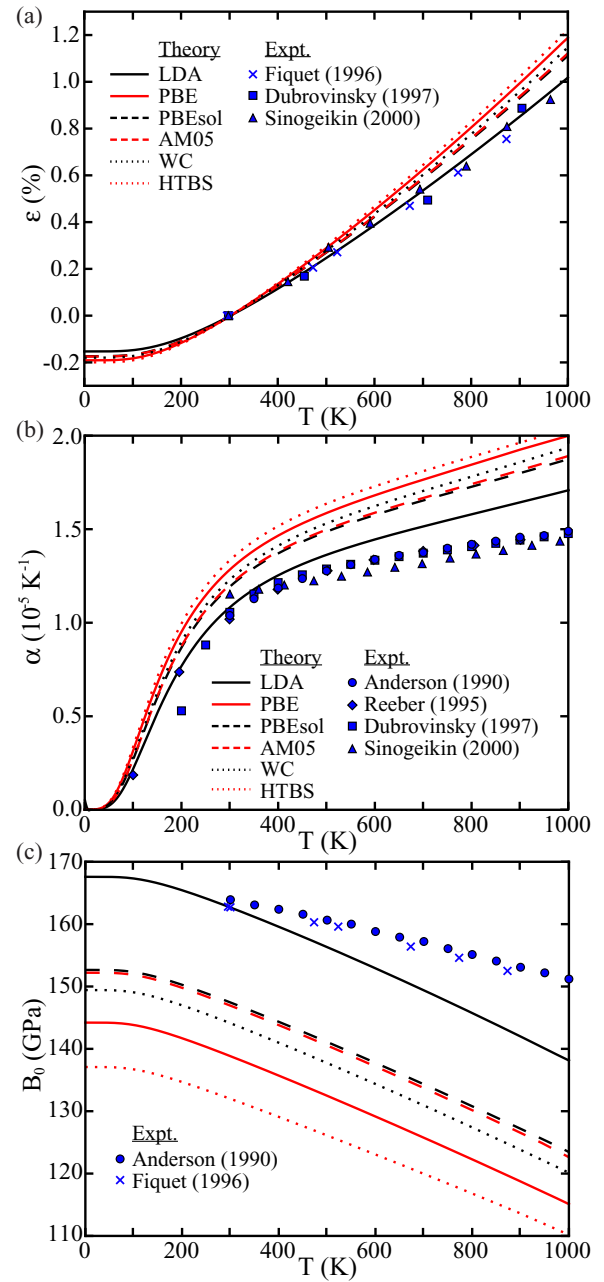

FIG. 10. (Color online) Variation of (a) the linear thermal expansion ε, (b) the coefficient of linear thermal expansion α, and (c) the bulk modulus B_0 of periclase as a function of the temperature computed using the different XC functionals: LDA in solid black, PBE in solid red (gray), PBEsol in dashed black, AM05 in dashed red (gray), WC in dotted black, and HTBS in dotted red (gray). Relevant experimental data are also reported. The labels correspond to the first author and year of publication of Refs. [60–64].

and the frequency of the IR-active mode ($\Delta\epsilon_m \propto \omega_m^{-2}$). As a result, the effects of the different XC functionals are closely connected to previous discussions of the structural properties and the frequencies at the Γ point. The largest differences (in absolute values [74]) from one functional to another obviously appear in the low frequency modes for which the contributions

TABLE XI. Electronic and static dielectric tensors of α-quartz, stishovite, zircon, and periclase. The contributions of the different phonon modes to the static dielectric tensor are also indicated. The tensors are all diagonal. For α-quartz, stishovite, and zircon, they have different components parallel ($\parallel$) and perpendicular ($\perp$) to the c axis, while the tensor is isotropic for periclase. In stishovite and zircon (respectively, α-quartz), the phonon mode contributions to $\epsilon_0^{\parallel}$ come from the three IR-active A_{2u} (respectively, A_2) modes, while the contributions to $\epsilon_0^{\perp}$ come from the four IR-active E_u (respectively, E) modes. In periclase, the contribution arises from the T_{1u} mode. For α-quartz, the experimental values (at 298 K) are taken from Ref. [32], except for the two lowest E modes which are from Ref. [69]. For stishovite, the measurements are those of Ref. [70]. For zircon, the reported experimental values are from Ref. [71] for the parallel components (values at 295 K), and from Ref. [72] for the perpendicular components. For periclase, the measurements are those of Ref. [73]. The "good" (absolute relative error smaller than 2%) theoretical values are in bold and the "bad" (absolute relative error larger than 5%) values are underlined.

	LDA	PBE	PBEsol	AM05	WC	HTBS	Expt.		LDA	PBE	PBEsol	AM05	WC	HTBS	Expt.
α-Quartz															
$\epsilon_\infty^{\parallel}$	2.50	**2.41**	**2.46**	**2.39**	**2.43**	2.31	2.42	$\epsilon_\infty^{\perp}$	2.47	**2.38**	**2.43**	**2.36**	**2.41**	2.29	2.39
$\Delta\epsilon_1^{\parallel}$	_0.73_	**0.68**	_0.71_	0.65	0.69	_0.00_	0.67	$\Delta\epsilon_1^{\perp}$	0.00	0.00	0.00	0.00	0.00	0.02	0.00
$\Delta\epsilon_2^{\parallel}$	_0.75_	_0.85_	_0.79_	_0.87_	_0.81_	_1.50_	0.65	$\Delta\epsilon_2^{\perp}$	_0.06_	_0.03_	0.05	_0.02_	_0.04_	_0.00_	0.05
$\Delta\epsilon_3^{\parallel}$	_0.15_	_0.05_	_0.09_	_0.04_	_0.07_	_0.00_	0.11	$\Delta\epsilon_3^{\perp}$	_0.41_	0.32	_0.36_	_0.31_	_0.35_	_0.00_	0.33
$\Delta\epsilon_4^{\parallel}$	_0.73_	_0.76_	_0.74_	_0.74_	_0.74_	_0.74_	0.66	$\Delta\epsilon_4^{\perp}$	**0.84**	_0.93_	_0.88_	_0.94_	_0.89_	_1.23_	0.83
								$\Delta\epsilon_5^{\perp}$	_0.03_	_0.01_	**0.02**	_0.01_	**0.02**	_0.00_	0.02
								$\Delta\epsilon_6^{\perp}$	_0.12_	**0.11**	**0.11**	**0.11**	**0.11**	_0.10_	0.11
								$\Delta\epsilon_7^{\perp}$	_0.70_	_0.72_	_0.71_	_0.71_	_0.71_	_0.71_	0.65
								$\Delta\epsilon_8^{\perp}$	**0.01**	_0.00_	**0.01**	_0.00_	**0.01**	_0.00_	0.01
$\epsilon_0^{\parallel}$	4.85	4.74	4.79	**4.68**	4.74	**4.55**	4.64	$\epsilon_0^{\perp}$	4.64	4.52	4.57	**4.46**	4.52	**4.35**	4.43
Stishovite															
$\epsilon_\infty^{\parallel}$	**3.38**	3.44	3.43	3.42	3.42	3.43	3.33	$\epsilon_\infty^{\perp}$	**3.30**	3.35	3.35	3.34	3.34	3.34	3.24
$\Delta\epsilon_1^{\parallel}$	5.59	5.77	5.63	5.60	5.69	5.62	–	$\Delta\epsilon_1^{\perp}$	6.85	9.01	7.49	7.69	7.58	7.67	–
								$\Delta\epsilon_2^{\perp}$	0.45	0.09	0.38	0.30	0.35	0.34	–
								$\Delta\epsilon_3^{\perp}$	0.79	0.74	0.80	0.78	0.79	0.79	–
$\epsilon_0^{\parallel}$	8.97	9.21	9.06	9.02	9.11	9.05	–	$\epsilon_0^{\perp}$	11.40	13.19	12.02	12.12	12.06	12.14	–
Zircon															
$\epsilon_\infty^{\parallel}$	_4.35_	_4.41_	_4.41_	_4.39_	_4.39_	_4.41_	3.80	$\epsilon_\infty^{\perp}$	_4.15_	_4.17_	_4.19_	_4.17_	_4.18_	_4.18_	3.50
$\Delta\epsilon_1^{\parallel}$	6.03	_7.12_	_6.53_	_6.71_	_6.49_	_6.69_	5.75	$\Delta\epsilon_1^{\perp}$	**5.69**	_8.07_	_6.68_	_7.15_	_6.59_	_7.10_	5.70
$\Delta\epsilon_2^{\parallel}$	_0.54_	_0.50_	_0.52_	_0.51_	_0.52_	_0.51_	0.36	$\Delta\epsilon_2^{\perp}$	_1.19_	_0.57_	_0.95_	_0.79_	_0.94_	_0.79_	0.60
$\Delta\epsilon_3^{\parallel}$	_0.88_	_0.95_	_0.91_	_0.92_	_0.91_	_0.91_	0.78	$\Delta\epsilon_3^{\perp}$	_0.12_	_0.23_	_0.17_	_0.20_	_0.16_	_0.21_	0.15
								$\Delta\epsilon_4^{\perp}$	_0.42_	_1.48_	_1.45_	_1.44_	_1.45_	_1.44_	1.20
$\epsilon_0^{\parallel}$	_11.80_	_12.98_	_12.37_	_12.54_	_12.30_	_12.51_	10.69	$\epsilon_0^{\perp}$	_12.59_	_14.52_	_13.44_	_13.76_	_13.31_	_13.70_	11.25
Periclase															
ϵ_∞	3.04	_3.10_	_3.11_	3.09	3.09	_3.10_	2.95								
$\Delta\epsilon$	_6.76_	_7.37_	_6.81_	_6.87_	_6.80_	_7.50_	6.25								
ϵ_0	_9.80_	_10.47_	_9.91_	_9.96_	_9.89_	_10.60_	9.20								
MRE (%)								MARE (%)							
ϵ_∞	6.59	6.59	7.27	6.10	6.68	5.42		ϵ_∞	6.59	6.83	7.27	6.81	6.68	7.91	
ϵ_0	7.62	13.70	9.86	9.88	9.01	10.05		ϵ_0	7.62	13.70	9.86	9.88	9.01	11.55	

can be quite significant (since $\Delta\epsilon_m \propto \omega_m^{-2}$). For such modes, the errors with respect to experiments can also be quite large.

For instance, the error on $\Delta\epsilon_1^{\perp}$ for zircon is about 40% when using PBE. It is also the contribution for which there is the largest difference between XC functionals (42% from LDA which is very close the experimental value to PBE). The difference in $\Delta\epsilon_m$ is the combination of the differences in each of its components (Ω_0, S_m, and ω_m). In this case, the most important differences originate from oscillator strength S_m (22%) and ω_m (12%, which also leads to 22% discrepancy when taken to the square). These are slightly compensated by the difference in Ω_0 (2%).

It is worth mentioning that the differences in the oscillator strength are due essentially to differences in the atomic displacements (related to the second derivatives of the total energy with respect to atomic displacements, just like the

frequencies). Indeed, we found that the XC functional has a very little impact (at most 1%–2%) on the Born effective charges (connected to the mixed second-order derivative of the energy with respect to atomic displacements and macroscopic electric field). And, since our results are in excellent agreement with previous calculations, the Born effective charges are not reported here for sake of brevity. However, we would like to point out that it is known that DFT tends to overestimate the Born effective charges [75], and, as a result, part of the discrepancy of $\Delta\epsilon_m$ with respect to experiments can be explained by the too large oscillator strengths.

Finally, we turn to the static dielectric constant ϵ_0. The theoretical values are larger than the experimental ones by about 8%–14%. This is directly related to previous discussion about ϵ_∞ and $\Delta\epsilon_m$. The best results are obtained within LDA, while PBE and HTBS lead to the worst results. The other three
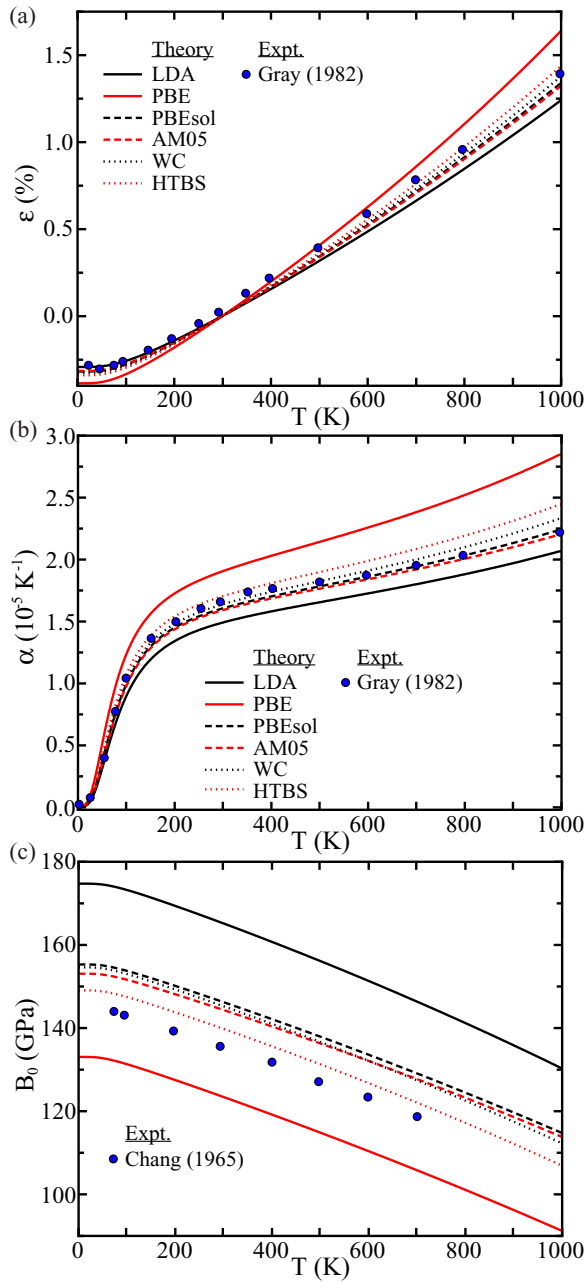
FIG. 11. (Color online) Variation of (a) the linear thermal expansion ε, (b) the coefficient of linear thermal expansion α, and (c) the bulk modulus B_0 of copper as a function of the temperature computed using the different XC functionals: LDA in solid black, PBE in solid red (gray), PBEsol in dashed black, AM05 in dashed red (gray), WC in dotted black, and HTBS in dotted red (gray). Relevant experimental data are reported. The labels correspond to the first author and year of publication of Refs. [65,66].

functionals (PBEsol, AM05, and WC) have a similar accuracy which is slightly worse than for LDA.

IV. DISCUSSION

In view of our results on different functionals, materials and DFPT properties, a few general statements and considerations can be made. For all oxides and semiconductors, LDA performs surprisingly well in most of the cases. As the LDA lattice parameter is strongly underestimated and the lattice parameter has a large role in determining the frequencies (see Sec. III D), the success of LDA must be due to some cancellation of errors. Accurate vibrational properties are obtained with a significantly underestimated lattice parameter. This implies that using the experimental lattice parameter with LDA will degrade the quality of the DFPT results. Interestingly, PBE does not benefit from a similar effect and, as a result, it is inaccurate in both the lattice parameters and the frequencies. Similar conclusions were found when investigating the theoretical Debye-Waller factors [18], leading the proposal of an *ad hoc* functional obtained by mixing 50% of LDA and 50% of PBE. The optimal functionals providing both accurate structural factors and reasonably accurate (i.e., at least better than PBE) frequencies are the WC, PBEsol, and AM05. Finally, HTBS is not to be recommended for DFPT as both structural parameters and frequencies are not accurate.

If one uses a functional such as PBEsol or WC (that give very good structural parameters), phonon frequencies are usually accurate within maximum 5%, vibrational entropies within maximum 6%, and static dielectric constants overestimate experiments systematically by at most 10%. These results show that while there are differences between functionals, DFPT computations are accurate enough to lead to a reasonable predictive power.

On the other hand, the only metal in our data set (copper) shows a very different behavior with the best functional being PBE and the worst being LDA, PBEsol, WC, and AM05. In view of previous work on metal phonon frequencies [19] and Debye-Waller factors [18] with DFPT, this discrepancy might originate from the pseudopotential.

V. SUMMARY

In this paper, the validity of various exchange-correlation functionals (LDA, PBE, PBEsol, WC, AM05, and HTBS) has been investigated for computing the structural, vibrational, dielectric, and thermodynamical properties of various materials (silicon, SiO_2 α-quartz and stishovite, $ZrSiO_4$ zircon, MgO periclase, and copper) in the framework of DFPT. For the structural properties, PBEsol and WC are found to provide the results closest to the experiments and AM05 performs only slightly worse. These three functionals constitute an improvement over LDA and PBE in contrast with HTBS, which has been shown to be really problematic for α-quartz.

For the vibrational and thermodynamical properties, LDA performs surprisingly very well. In the majority of cases, it outperforms PBE significantly and yields slightly better results than the WC, PBEsol, and AM05 functionals. For the latter functionals, this slight improvement is however detrimental for the structural parameters. On the other hand, HTBS performs also poorly for vibrational quantities.

For the dielectric properties, all the functionals fail to reproduce the electronic dielectric constant due to the well-known band-gap problem. They all tend to overestimate the oscillator strengths and hence the static dielectric constant.

Overall, LDA provides very good performances in DFPT computations provided the LDA lattice parameter is used. If accurate lattice parameters are also sought for, the PBEsol, WC,

and AM05 provide the most accurate structural results while still improving in terms of vibrational quantities compared to PBE. These conclusions would definitely be strengthened by considering a larger number of materials, and by performing some all-electron calculations for the dynamical properties.

[1] R. P. Feynman, in *Six Easy Pieces* (Addison-Wesley, Reading MA, 1991), p. 59.

[2] G. Hautier, A. Jain, and S. P. Ong, J. Mater. Sci. **47**, 7317 (2012).

[3] W. Kohn and L. J. Sham, Phys. Rev. **140**, A1133 (1965).

[4] S. Baroni, S. de Gironcoli, A. Dal Corso, and P. Giannozzi, Rev. Mod. Phys. **73**, 515 (2001).

[5] J. P. Perdew and Y. Wang, Phys. Rev. B **45**, 13244 (1992).

[6] J. P. Perdew, K. Burke, and M. Ernzerhof, Phys. Rev. Lett. **77**, 3865 (1996).

[7] R. Armiento and A. E. Mattsson, Phys. Rev. B **72**, 085108 (2005).

[8] W. Kohn and A. E. Mattsson, Phys. Rev. Lett. **81**, 3487 (1998).

[9] J. P. Perdew, A. Ruzsinszky, G. I. Csonka, O. A. Vydrov, G. E. Scuseria, L. A. Constantin, X. Zhou, and K. Burke, Phys. Rev. Lett. **100**, 136406 (2008).

[10] Z. Wu and R. E. Cohen, Phys. Rev. B **73**, 235116 (2006).

[11] P. Haas, F. Tran, and P. Blaha, Phys. Rev. B **79**, 085104 (2009).

[12] P. Haas, F. Tran, P. Blaha, and K. Schwarz, Phys. Rev. B **83**, 205117 (2011).

[13] B. Hammer, L. B. Hansen, and J. K. Nørskov, Phys. Rev. B **59**, 7413 (1999).

[14] F. Favot and A. Dal Corso, Phys. Rev. B **60**, 11427 (1999).

[15] A. Dal Corso and S. de Gironcoli, Phys. Rev. B **62**, 273 (2000).

[16] B. Grabowski, T. Hickel, and J. Neugebauer, Phys. Rev. B **76**, 024309 (2007).

[17] K. Hummer, J. Harl, and G. Kresse, Phys. Rev. B **80**, 115205 (2009).

[18] F. D. Vila, J. J. Rehr, H. H. Rossner, and H. J. Krappe, Phys. Rev. B **76**, 014301 (2007).

[19] A. Dal Corso, J. Phys.: Condens. Matter **25**, 145401 (2013).

[20] X. Gonze *et al.*, Comput. Phys. Commun. **180**, 2582 (2009); http://www.abinit.org

[21] M. A. L. Marques, M. J. T. Oliveira, and T. Burnus, Comput. Phys. Commun. **183**, 2272 (2012); http://www.tddft.org/programs/Libxc

[22] M. Oliveira and F. Nogueira, Comput. Phys. Comm. **178**, 524 (2008); http://www.tddft.org/programs/APE/.

[23] *Landolt-Börnstein Semiconductors*, edited by O. Madelung, U. Rössler, and M. Schulz (Springer-Verlag, Berlin, Heidelberg, New York, 2002), Vol. 41.

[24] L. Levien, C. T. Prewitt, and D. Weidner, Am. Mineral. **65**, 920 (1980).

[25] R. J. Hill, M. D. Newton, and G. V. Gibbs, J. Solid State Chem. **47**, 185 (1983).

[26] Z. Mursic, T. Vogt, H. Boysen, and F. Frey, J. Appl. Crystallogr. **25**, 519 (1992).

[27] B. Li, K. Woody, and J. Kung, J. Geophys. Res. **111**, B11206 (2006).

[28] N. W. Ashcroft and N. D. Mermin, *Solid State Physics* (Saunders College, Philadelphia, 1976).

[29] W. G. Wyckoff, *Crystal Structures*, 4th ed. (Interscience, New York, 1974).

[30] The Born effective charge tensors ($Z^*_{ij,\tau}$) are defined as the force in the direction i on the atom τ due to an homogeneous unitary electric field along the direction j, or equivalently, as the induced polarization of the solid along the direction i by a unit displacement in the direction j of the sublattice generated by atom τ. The Born effective charge tensors govern, with the electronic permittivity tensor ϵ_∞, the strength of Coulomb interaction responsible of the splitting between the longitudinal (LO) and transverse (TO) optic modes. For the sake of brevity, the calculated Born effective charge tensors are not reported here. In fact, we found that the XC functionals provide very similar results.

[31] G. Dolling, in *Inelastic Scattering of Neutrons in Solids and Liquids*, edited by S. Ekland (IAEA, Vienna, 1963), Vol. II, p. 37.

[32] F. Gervais and B. Piriou, Phys. Rev. B **11**, 3944 (1975).

[33] E. K. Zakharova, V. G. Zubov, and L. P. Osipova, Kristallografiya **19**, 788 (1974) [Sov. Phys. Crystallogr. **19**, 489 (1975)].

[34] M. F. Vigasina, E. V. Guseva, and R. Y. Orlov, Fiz. Tverd. Tela/Phys. Solid State **31**, 47 (1989).

[35] A. M. Hofmeister, J. Xu, and S. Akimoto, Am. Mineral. **75**, 951 (1990).

[36] P. Dawson, M. M. Hargreave, and G. R. Wilkinson, J. Phys. C: Solid State Phys. **4**, 240 (1971).

[37] M. J. L. Sangster, G. Peckham, and D. H. Saunderson, J. Phys. C **3**, 1026 (1970).

[38] G. Nilsson and G. Nelin, Phys. Rev. B **6**, 3777 (1972).

[39] B. Dorner, H. Grimm, and H. Rzany, J. Phys. C **13**, 6607 (1980).

[40] D. Strauch and B. Dorner, J. Phys.: Condens. Matter **5**, 6149 (1993).

[41] H. Schober *et al.*, J. Phys.: Condens. Matter **5**, 6155 (1993).

[42] A. Bosak *et al.*, Geophys. Res. Lett. **36**, L19309 (2009).

[43] R. Mittal, S. L. Chaplot, M. N. Rao, N. Choudhury, and R. Parthasarthy, Physica B **241**, 403 (1998).

[44] R. Mittal, S. L. Chaplot, R. Parthasarathy, M. J. Bull, and M. J. Harris, Phys. Rev. B **62**, 12089 (2000).

[45] S. L. Chaplot, L. Pintschovius, N. Choudhury, and R. Mittal, Phys. Rev. B **73**, 094308 (2006).

[46] E. C. Svensson, B. N. Brockhouse, and J. M. Rowe, Phys. Rev. **155**, 619 (1967).

[47] R. M. Nicklow, G. Gilat, H. G. Smith, L. J. Raubenheimer, and M. K. Wilkinson, Phys. Rev. **164**, 922 (1967).

[48] S. Ganesan, Philos. Mag. **7**, 197 (1962).

[49] H. Ledbetter, Int. J. Thermophys. **12**, 637 (1991).

[50] J. G. Collins, Philos. Mag. **8**, 323 (1963).

[51] K. A. Gschneider, Jr., in *Solid State Physics*, edited by F. Seitz and D. Turnbull (Academic, New York, 1964), Vol. 16, p. 275.

[52] C. Lee and X. Gonze, Phys. Rev. B **51**, 8610 (1995).

[53] M. W. Chase, *NIST-JANAF Thermochemical Tables* (American Institute of Physics, Woodbury, NY, 1998).

[54] O. Kubaschewski, C. B. Alcock, and P. J. Spencer, in *Materials Thermochemistry*, 6th ed. (Pergamon, New York, 1993), Chap. 5, pp. 257–323.

[55] W. Yong, E. Dachs, A. Benisek, and R. A. Secco, Phys. Chem. Minerals **39**, 153 (2012).

[56] Given the good agreement between the calculated and experimental phonon band structures, we suspect a problem with the experimental measurement.

[57] S. Lany, Phys. Rev. B **78**, 245207 (2008).

[58] G. Hautier, S. P. Ong, A. Jain, C. J. Moore, and G. Ceder, Phys. Rev. B **85**, 155208 (2012).

[59] F. Birch, Phys. Rev. **71**, 809 (1947).

[60] O. Anderson and K. Zou, J. Phys. Chem. Ref. Data **19**, 69 (1990).

[61] R. R. Reeber, K. Goessel, and K. Wang, Eur. J. Mineral. **7**, 1039 (1995).

[62] G. Fiquet, D. Andrault, J. P. Itié, P. Gillet, and P. Richet, Phys. Earth Planet. Inter. **95**, 1 (1996).

[63] L. S. Dubrovinsky and S. K. Saxena, Phys. Chem. Miner. **24**, 547 (1997).

[64] S. V. Sinogeikin, J. M. Jackson, B. O'Neill, J. W. Palko, and J. D. Bass, Rev. Sci. Instrum. **71**, 201 (2000).

[65] Y. A. Chang and R. Hultgren, J. Phys. Chem. **69**, 4162 (1965).

[66] *American Institute of Physics Handbook*, 3rd ed., edited by E. D. Gray (McGraw-Hill, New York, 1982).

[67] A. Otero-de-la-Roza and V. Luaña, Phys. Rev. B **84**, 024109 (2011).

[68] D. Zhang and J.-X. Sun, Chinese Phys. B **21**, 080508 (2012).

[69] E. E. Russel and E. E. Bell, J. Opt. Soc. Am. **57**, 341 (1967).

[70] S. M. Stishov and S. V. Popova, Geokhimiya **10**, 837 (1961).

[71] F. Gervais, B. Piriou, and F. Cabannes, J. Phys. Chem. Solids **34**, 1785 (1973).

[72] C. Pecharromán, M. Ocaña, P. Tartaj, and C. J. Serna, Mater. Res. Bull. **29**, 417 (1994).

[73] T. Sun, P. B. Allen, D. G. Stahnke, S. D. Jacobsen, and C. C. Homes, Phys. Rev. B **77**, 134303 (2008).

[74] For high-frequency modes, the relative errors with respect to experiments and the relative difference from one functional to another can be enormous due to the small absolute values of the contributions. This is the case of $\Delta\epsilon_8^\perp$ in α-quartz, for example.

[75] A. Filippetti and N. A. Spaldin, Phys. Rev. B **68**, 045111 (2003).